CDF Note 10423

Measurement of the $W \to \ell\nu + \geq n$ jets Cross Section

The CDF Collaboration
(http://www-cdf.fnal.gov)

June 13, 2012

Abstract

In this note we document the measurement of $W + n$ jets. Outside the EWK properties the W, we examine jet kinematic variables in an effort to study pQCD predictions at high momentum transfer. We derive several differential cross sections corrected to the hadron level such as the inclusive jet multiplicity and the nth leading jet p_T for each inclusive n jet. We also consider cross sections normalized to the total integrated (inclusive jet multiplicity) cross section as well as additional cross section ratios. In this analysis, we are using 2.8 fb^{-1} of data and consider both the electron and muon lepton final states for the W decay.

I Introduction

The study of the kinematic properties of jets associated with a heavy vector boson (W or Z) provides a window into better understanding theoretical perturbative QCD (Quantum Chromodynamics) predictions. In particular, the leptonic decay allows for a clean "tag" of an event with high momentum transfer and therefore, this process allows access to a region of interest purely from a SM measurement prospective. However, the production of W+jets is of special interest to $t\bar{t}$, Higgs (in the relevant decay channels), and beyond the standard model processes that have W+jets as a background that needs to be well understood.

This note presents cross section as well as ratio cross section results for both $W \to e\nu$ and $W \to \mu\nu$ decay channels for $\geq$1 to $\geq$4 jets. These observables are defined and presented in the last section of this note. This work is an update and expansion of the previous analysis using 320 pb^{-1} [1]. For this analysis, we utilized 2.8 fb^{-1} of data via a high transverse momentum (track $p_T > 18$ GeV/c) trigger using the CDF II detector.

The organization of this note is a follows. We provide a short introduction to the CDF II Detector and CDF II coordinate system along with some useful variables in section II. Our W selection is discussed in section III. Then in section IV we give our jet definition and selection criteria. We provide a brief discussion of our background estimation as well as our combined luminosity acceptance, and efficiencies in sections V and VI, respectively. Section VII breaks down the various systematics uncertainties we calculate. Finally, in section VIII we provide a cornucopia of plots and tables for our cross section and cross section ratio measurements.

II CDF II Detector

CDF II is a general purpose azimuthally and forward-backward symmetric solenoidal detector located at the Tevatron $p\bar{p}$ collider at Fermilab. The detector consistence of precision charged particle tracking systems interior to fast projective calorimetry and fine grained muon detectors [2][3]. Tracking systems are contained in a superconducting solenoid, 1.5 m in radius and 4.8 m in length. This generates a 1.4 T magnetic field parallel to the beam axis. Calorimetry and muon systems are all outside the solenoid. The basic of design of the detector is to have multiple layers of individual sub-detectors that measure individual physical components of each event and from these infer type of particle and its kinematics.

The CDF II coordinate system is taken as in cylindrical coordinates (r, ϕ, z) which are useful in describing the detector geometry. The z axis is defined by the proton beam direction with r taken as the cylindrical radius from the beam pipe. The center of the detector is represented by r and z equal to zero while ϕ=0 points opposite of center of the Tevatron ring. However, for the purpose of describing particle trajectories and location, we use the spherical coordinates θ and ϕ as the polar and azimuthal angles, respectively, defied with respect to the z axis. The pseudorapidity, η, is defied as $\eta \equiv -\ln[\tan(\theta/2)]$. The transverse momentum of a particle is $p_T = p\sin\theta$ and its transverse energy is defined by $E_T = E\sin\theta$. Additionally in this note we take the distance between objects in the η-ϕ plane as ΔR defined as $\Delta R = \sqrt{(\Delta\eta)^2 + (\Delta\phi)^2}$ with $\Delta\eta$ and $\Delta\phi$ being the respective difference between the pseudorrapidities and azimuthal angles of the two objects.

III W Selection

Starting with our high transverse momentum sample, we apply various selection requirements in order to obtain our final W candidates. We first restrict our sample to leptons to be fiducial to the central region of our detector; effectively $|\eta| < 1.1$ for the pseudo-rapidity of the electron and muon. Both lepton channels are required to have well reconstructed tracks from our central drift chamber.

The tracking system provides the direction of the leptons, but the absolute value of their 3-momentum for electrons is determined from the energy deposited in the calorimeters. This energy is required to geometrically match the track and be consistent with that expected from electrons. For muons, we measure the momentum from the curvature of our tracks and require the energy deposited in the calorimeter to be consistent with a minimum ionizing particle. Using the respective transverse momentum of each charged lepton we require $p_T > 20$ GeV/c. We construct the missing energy ($\not\!\!E_T$) of the event by calculating a vector energy sum over all calorimeter towers and negating the quantity via conservation of energy. We do not directly apply a $\not\!\!E_T$ cut but rather apply a transverse mass cut: $M_T > 40$ for electrons and $M_T > 30$ for muons with

$$M_T = 2\sqrt{\left(p_T^{\ell}\, \not\!\!E_T\right)} \sin(\Delta\phi(\ell, \nu)/2)$$

Additional identification and quality cuts are applied to reject fakes and to better distinguish background from signal. In particular, we require that the excess calorimeter transverse energy deposited in a cone of $R = \sqrt{(\Delta\phi)^2 + (\Delta\eta)^2} = 0.4$ around each lepton be less than 10% of its transverse momentum. We also apply an additional isolation constraint such that the candidate lepton be well separated, $R > 0.52$ from the nearest jet in η-ϕ.

IV Jet Definition

Jets are constructed and defined using the cone-based Midpoint algorithm [4] using an η-ϕ cone radius of 0.4 ($R = 0.4$). Jets are selection with two cuts:

- $p_T \geq 20$ GeV/c
- $|\eta| \leq 2.0$

The pseudo-rapidity cut was chosen based on the understanding of the detector and the reliability of describing jet energy corrections at forward rapidity. The p_T cut was also similarly selected with the additional advantage being that a higher momentum jet definition selects against the effect of additional interactions. As noted in the previous section, we apply an additional event level cut which makes sure jets are well separated from the lepton ($R > 0.52$).

In addition to correcting the detector response [5], jets are corrected back to the hadron level using the same midpoint algorithm on the MC before CDF simulation. This hadron level "unfolding" correction is typically a bin-by-bin correction. We do not perform a parton level correction.

V Background Estimation

Our total background estimation is a composite of three different components. We estimate diboson (defined here as WW, WZ, and $W\gamma*$) and $t\bar{t}$ contributions by applying the known theoretical cross sections to MC. For our Z+jets and $W \to \tau\nu$+jets background we apply a scale factor based on M_T shape fitting to the data in order to avoid biasing the result. To do this, we also derive a sample and transverse mass profile based on a QCD/fake rich selection. This sample is comprised of events that match our W kinematic selection but fail a combination of two identification and quality requirements. The result of this procedure is a scale factor for each jet multiplicity for both the Z+jets and $W \to \tau\nu$+jets background as well as our QCD/fake backgrounds.

VI Luminosity, Acceptance, and Efficiencies

The denominator of our cross section definition involves the product of luminosity (2.8 fb^{-1}), acceptance, and efficiency. We calculate our analysis efficiency via a data driven method and the results represent the total efficiency of our selection criteria that cannot be directly estimated from MC/simulation. This includes our tracking, quality, identification, reconstructed, and trigger, etc. requirements. The acceptance represents the fraction of signal MC events passing our W kinematic selection. The acceptance is calculated for each lepton channel and for each inclusive jet multiplicity 0-4.

For the purpose of comparison to theory results we redefine our cross section via a restricted or "reduced" acceptance by applying our basic W selection cuts at generator level to our W signal/acceptance MC (as described in section III). These post final state radiation lepton cuts are summarized in table 1.

$W \to e\nu$	$W \to \mu\nu$
$\lvert\eta_e\rvert \leq 1.1$	$\lvert\eta_\mu\rvert \leq 1.0$
$p_T^e \geq 20$ GeV/c	$p_T^\mu \geq 20$ GeV/c
$M_T^W \geq 40$ GeV/c^2	$M_T^W \geq 30$ GeV/c^2

Table 1: W generator level cuts used in our redefined cross section with reduced acceptance. We use the *post* final state radiation lepton for our cuts. The electron and muon channels are nearly identical with exception to tighter M_T cut on the electrons relative to the muons.

VII Systematic Uncertainties

We consider several different sources of systematic uncertainty which we outline here. These uncertainties in addition to the normal statistical uncertainty.

For our absolute cross section measurements we include a global independent systematic uncertainty for the luminosity of 5.8%. We will quote this systematic as separate from the total of our other systematic uncertainties and note that this systematic completely cancels in any type of cross section ratio.

Then there are systematic uncertainties that relate to our understanding of our acceptance which include our choice of parton density functions (PDFs) and handling of final state radiation (FSR). We also assign a systematic to our understanding and reweighting correction of the number of vertices in the event. Each of these three systematic uncertainties are calculated for each lepton (electron and muon) channel and for each inclusive jet multiplicity. Like our luminosity systematic uncertainty, these systematics completely cancel for cross section ratios between the same jet multiplicity and channel.

We then have several uncertainties contributions that are dependent on our jet kinematic variables (e.g. jet p_T). First we have two systematic uncertainties related to our background estimation which concern with our template fitting procedure as well as our understanding of our diboson and $t\bar{t}$ cross section. Finally we apply two sets of systematic uncertainties related to our jets corrections. One of these relates to the detector level energy scale corrections we apply while the other is our systematic uncertainty due to correcting our cross sections back to the hadron level.

After accounting for the correlation in our final jet level corrections and taking our remaining systematics as uncorrelated we arrive at our total systematic uncertainty. As noted we will denote the systematic uncertainty in terms of the universal luminosity systematic and combine all other systematics. These systematic uncertainties as well as the error from the statistics of the cross section form our total uncertainty.

We also note that we also consider additional cross section ratios and normalized cross section shapes. For these observables, we necessarily take into account the various correlations between quantities. This leads into a reduction of the systematics uncertainties and thus a tighter handle to constrain theoretical predictions.

VIII Results

For a generic differential cross section, $\mathrm{d}\sigma/\mathrm{d}f$, the cross section is defined as

$$\frac{\mathrm{d}\sigma}{\mathrm{d}f} = u\left(\frac{N_{data} - N_{bkgd}}{LA\epsilon}\right)$$

where $u = u(f)$ is the jet hadron level correction, N_{data} is number of candidate events in data, N_{bkgd} is the number of background events estimated, L is the integrated luminosity, A is the W+jets acceptance, ϵ is the total efficiency.

Our analysis includes several differential cross sections which are defined in each subsection. For the results presented in this note, we use our signal MC (Alpgen v2.10 [6] with Pythia v6.325 [7]) as our on plot theory prediction.

Jet Multiplicity: $\frac{\mathrm{d}\sigma}{\mathrm{d}n} = \sigma_n$

We measure the inclusive jet multiplicity cross-section for up to $\geq$4 jets. In addition, we make the same distribution but with each bin/multiplicity normalized to the total inclusive W cross-section (σ_0).

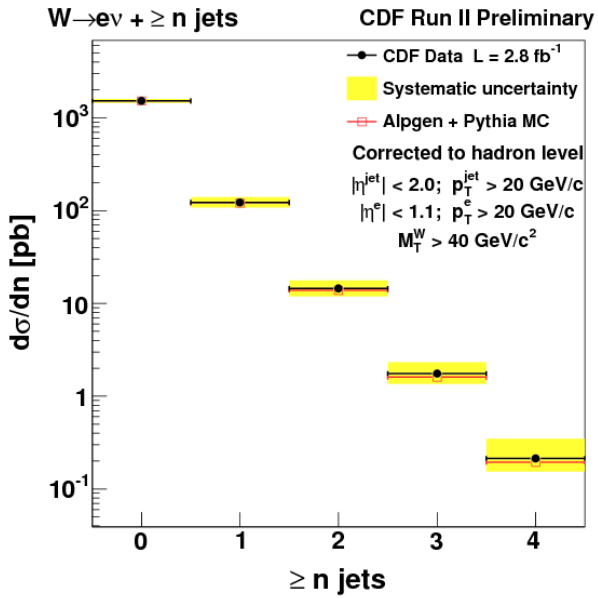

Figure 1: $W \to e\nu$ jet multiplicity.

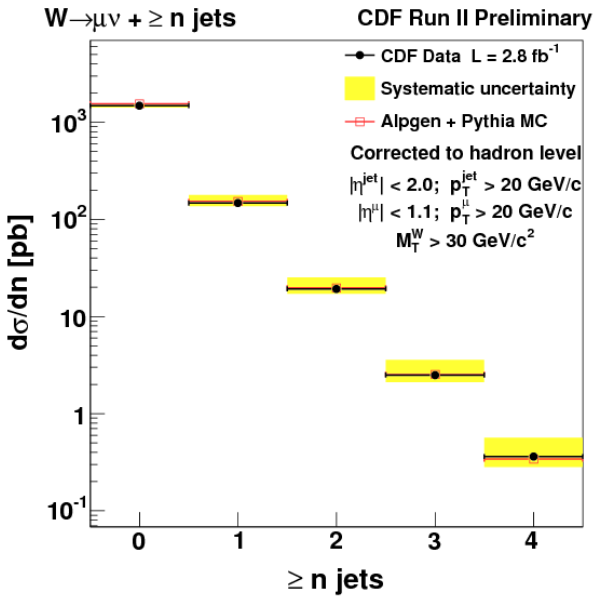

Figure 2: $W \to \mu\nu$ jet multiplicity.

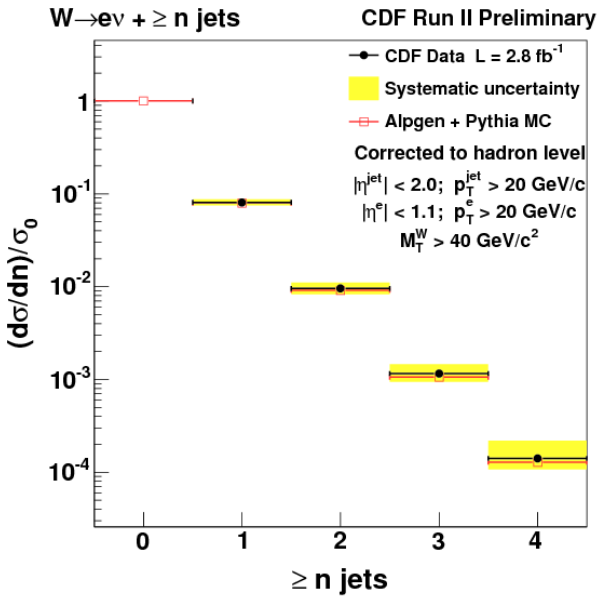

Figure 3: $W \to e\nu$ jet multiplicity normalized to the total inclusive $W \to e\nu$ cross section.

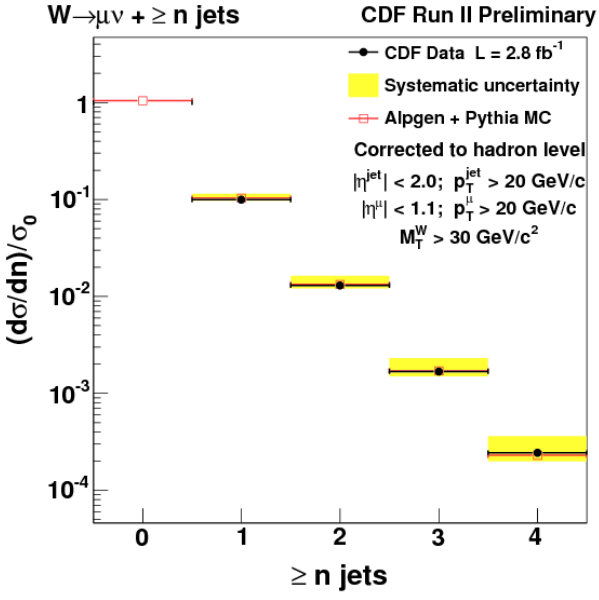

Figure 4: $W \to \mu\nu$ jet multiplicity normalized to the total inclusive $W \to \mu\nu$ cross section.

Jet Multiplicity Ratio: $\frac{\sigma_{n+1}}{\sigma_n}$

We form a ratio quantity with the n+1 jet multiplicity cross-section divided by the n jet cross-section (σ_{n+1}/σ_n).

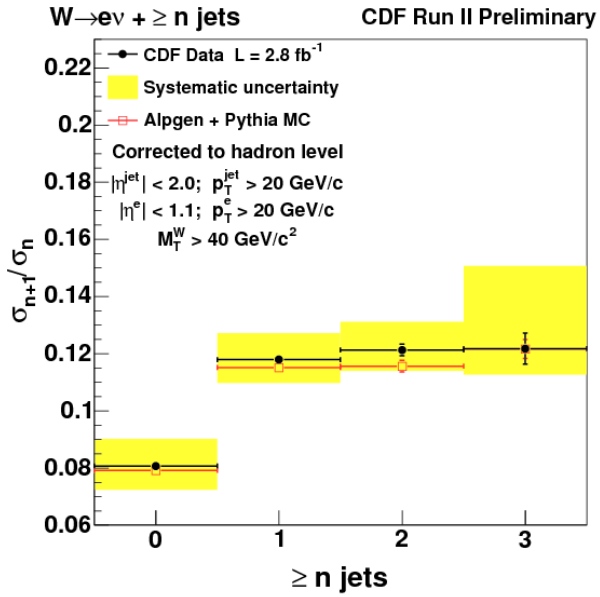

Figure 5: $W \to e\nu$ σ_{n+1}/σ_n.

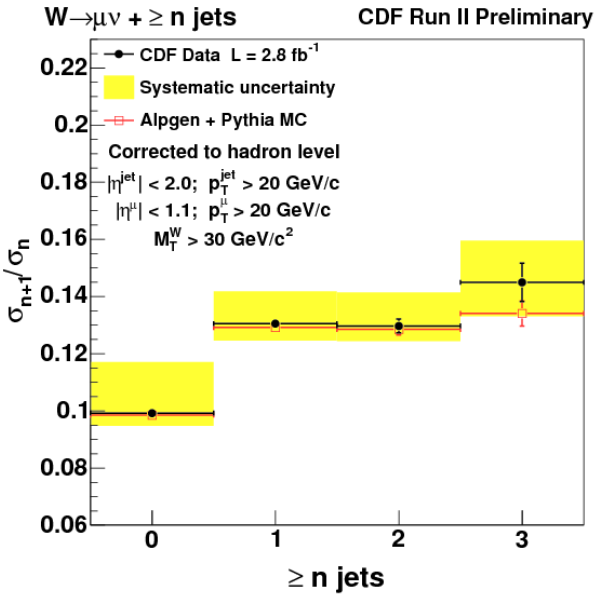

Figure 6: $W \to \mu\nu$ σ_{n+1}/σ_n.

n^{th} Leading Jet p_T: $\frac{\mathrm{d}\sigma_n}{\mathrm{d}p_T^{n\text{th}}}$

For $\geq n$ jets we measure the jet p_T of the n^{th} leading jet for 1-4 jets. With this differential cross-section, we also make a data/theory comparison using W+jets Alpgen+Pythia MC for our theory prediction.

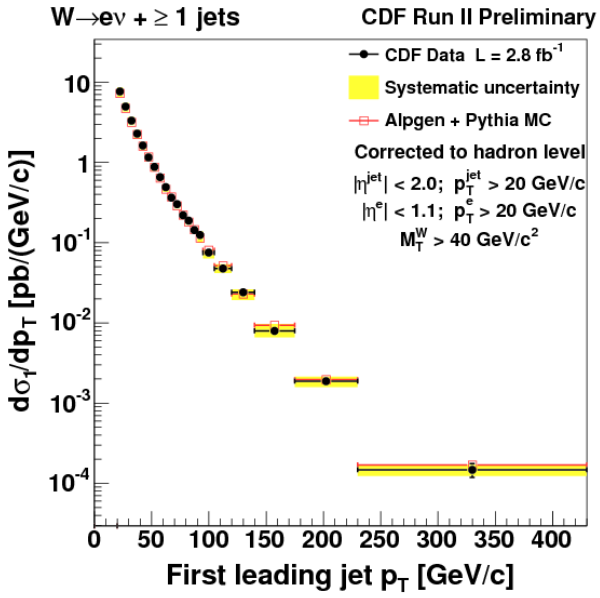

Figure 7: First leading jet p_T for $W \to e\nu + \geq 1$ jet.

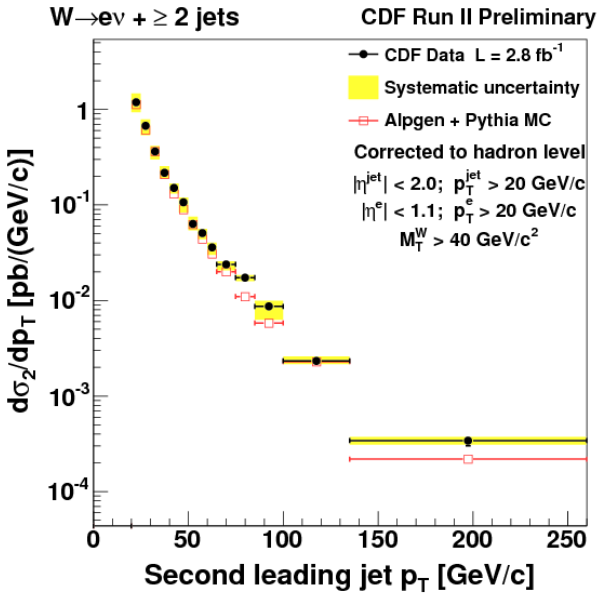

Figure 8: 2^{nd} leading jet p_T for $W \to e\nu + \geq 2$ jets.

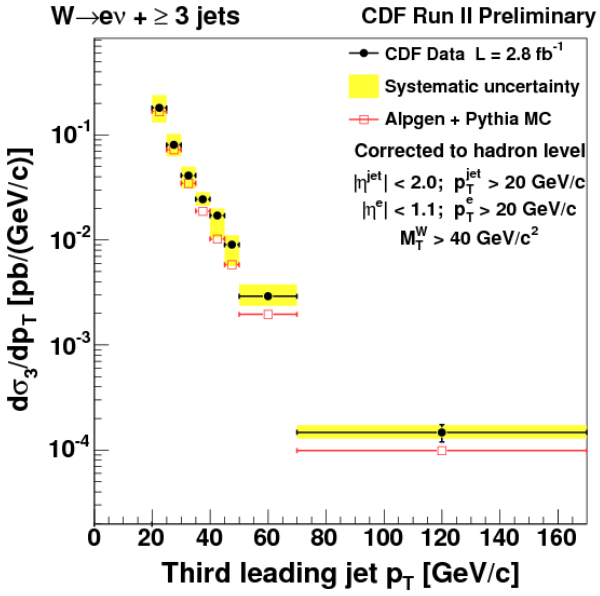

Figure 9: 3^{rd} leading jet p_T for $W \to e\nu + \geq 3$ jets.

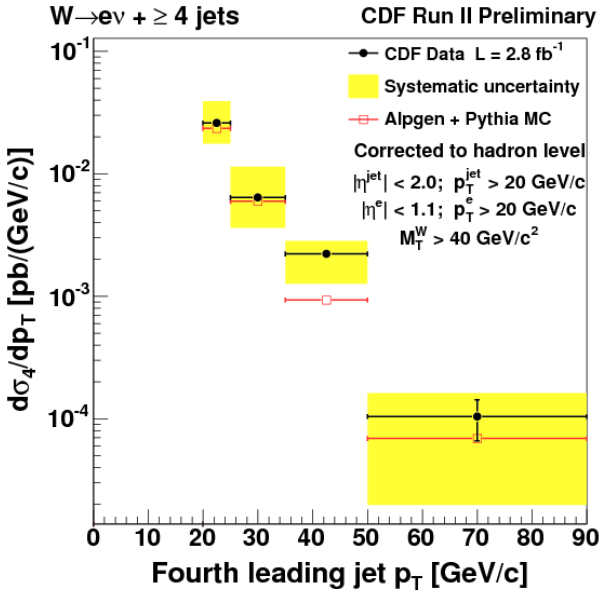

Figure 10: 4^{th} leading jet p_T for $W \to e\nu + \geq 4$ jets.

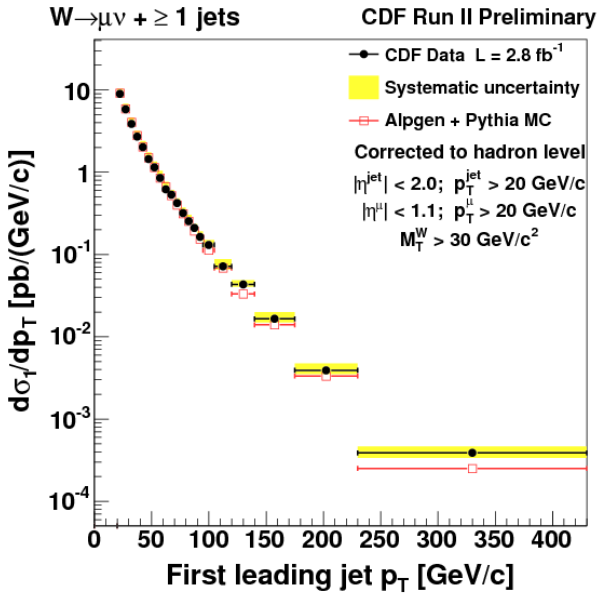

Figure 11: First leading jet p_T for $W \to \mu\nu + \geq 1$ jet.

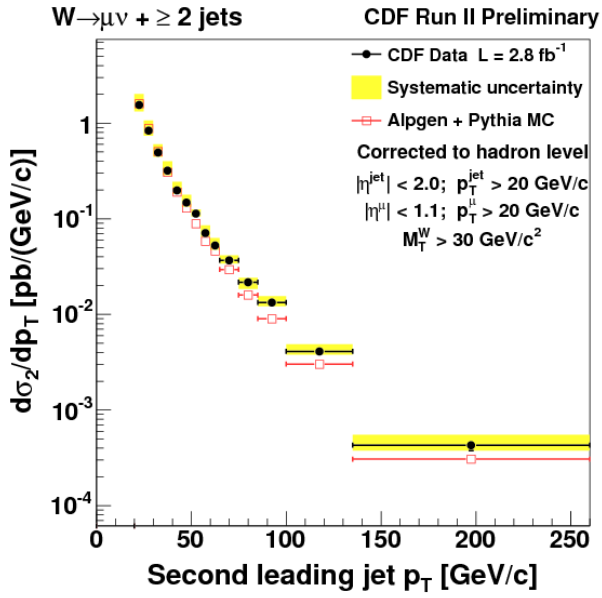

Figure 12: 2^{nd} leading jet p_T for $W \to \mu\nu + \geq 2$ jets.

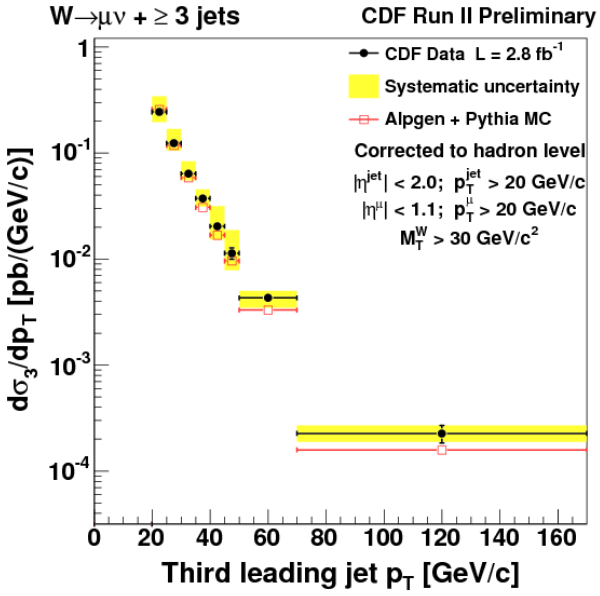

Figure 13: 3^{rd} leading jet p_T for $W \to \mu\nu + \geq 3$ jets.

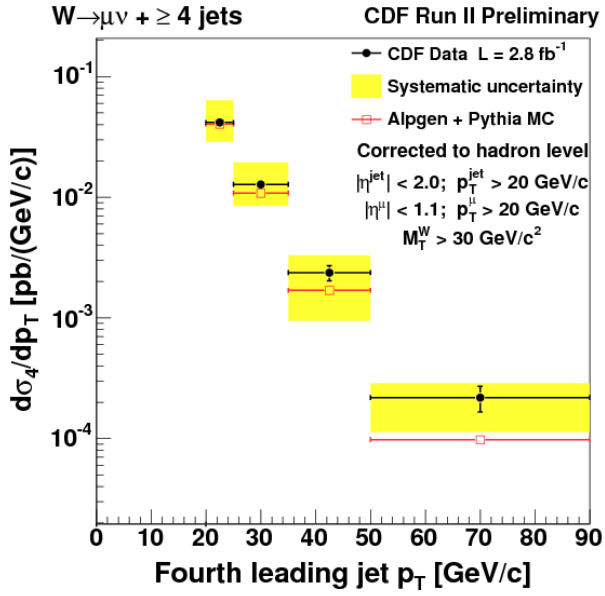

Figure 14: 4^{th} leading jet p_T for $W \to \mu\nu + \geq 4$ jets.

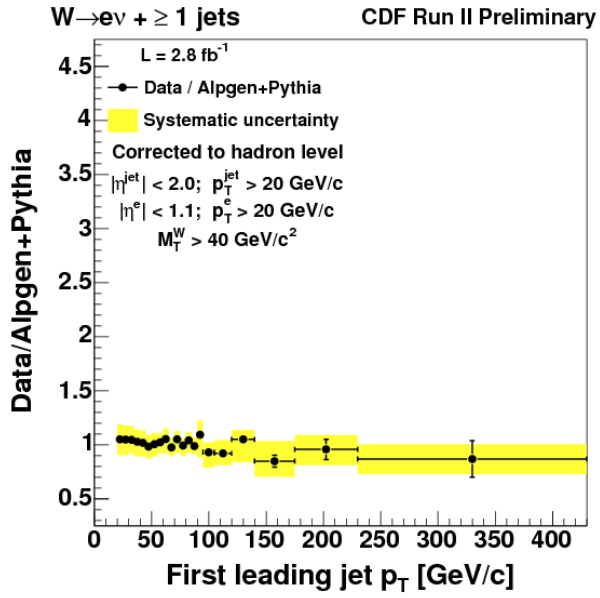

Figure 15: Data/Theory First leading jet p_T for $W \to e\nu + \geq 1$ jet.

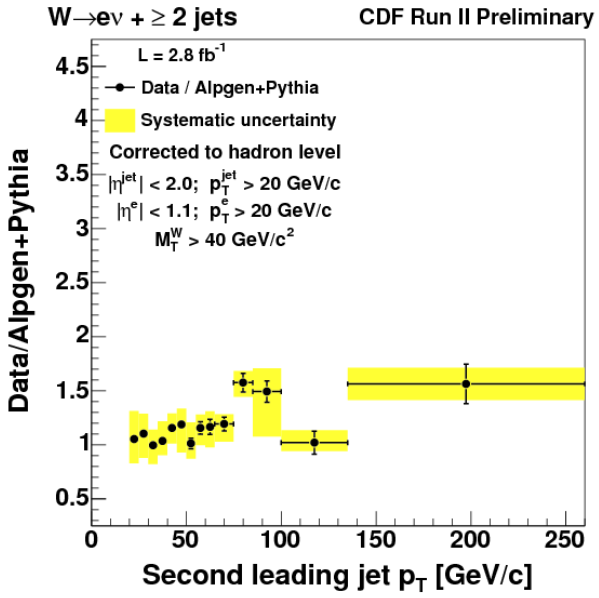

Figure 16: Data/Theory 2$^{\text{nd}}$ leading jet p_T for $W \to e\nu + \geq 2$ jets.

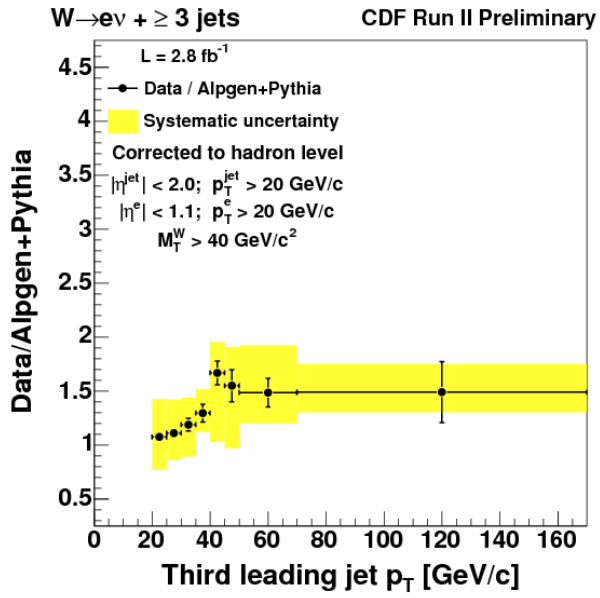

Figure 17: Data/Theory 3$^{\text{rd}}$ leading jet p_T for $W \to e\nu + \geq 3$ jets.

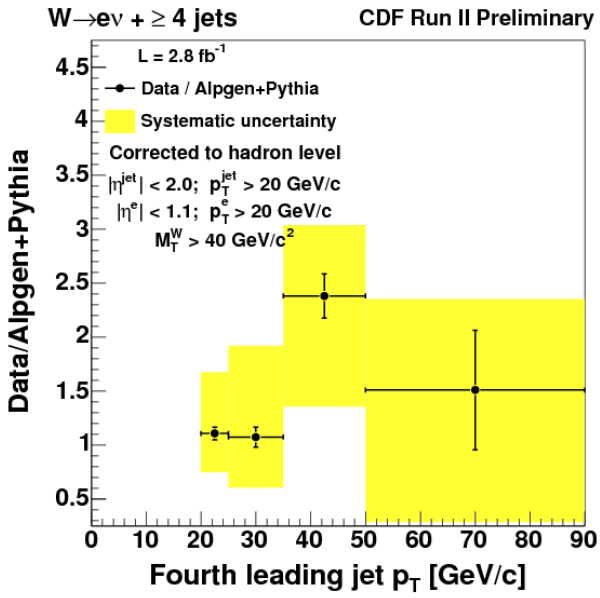

Figure 18: Data/Theory 4$^{\text{th}}$ leading jet p_T for $W \to e\nu + \geq 4$ jets.

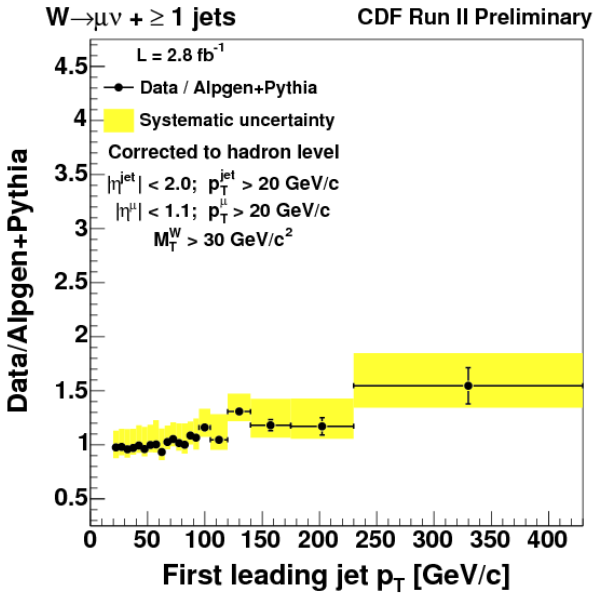

Figure 19: Data/Theory First leading jet p_T for $W \to \mu\nu + \geq 1$ jet.

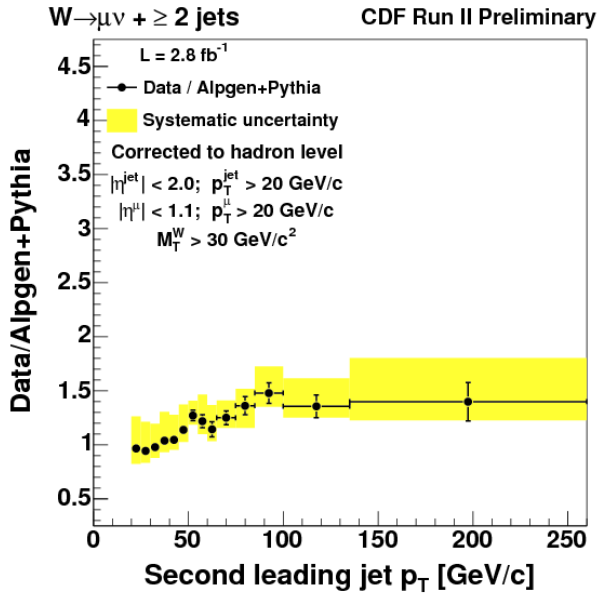

Figure 20: Data/Theory 2$^{\text{nd}}$ leading jet p_T for $W \to \mu\nu + \geq 2$ jets.

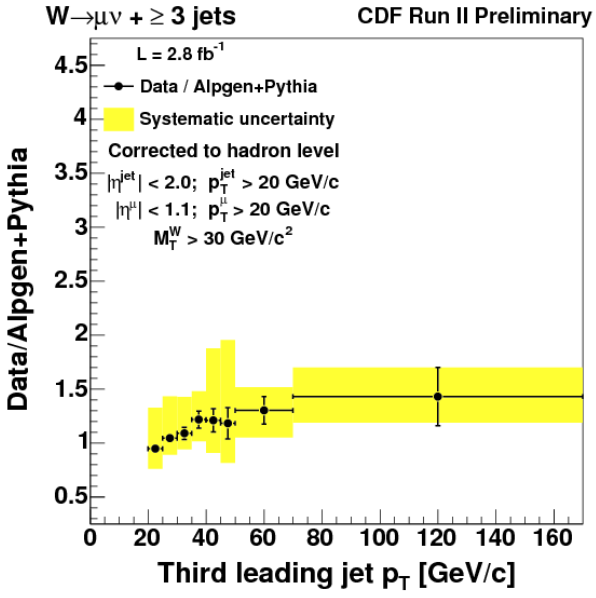

Figure 21: Data/Theory 3$^{\text{rd}}$ leading jet p_T for $W \to \mu\nu + \geq 3$ jets.

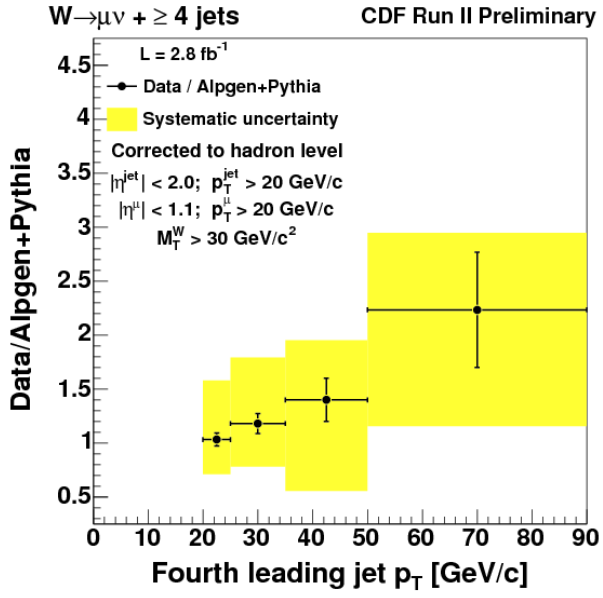

Figure 22: Data/Theory 4$^{\text{th}}$ leading jet p_T for $W \to \mu\nu + \geq 4$ jets.

Dijet Mass and Separation: $\frac{d\sigma_2}{dm_{jj}}$ & $\frac{d\sigma_2}{dR_{jj}}$

Using the two leading (highest p_T jets) we calculate the dijet mass (m_{jj}) and dijet separation (R_{jj}) in η-ϕ.

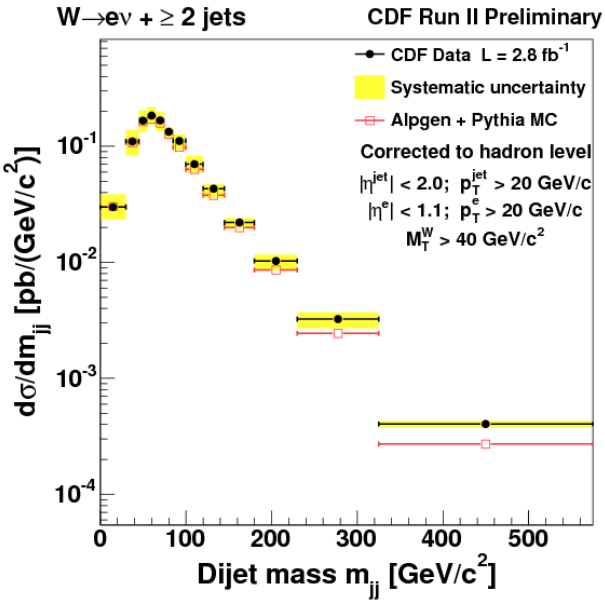

Figure 23: Dijet Mass Cross-section for $W \to e\nu + \geq 2$ jets.

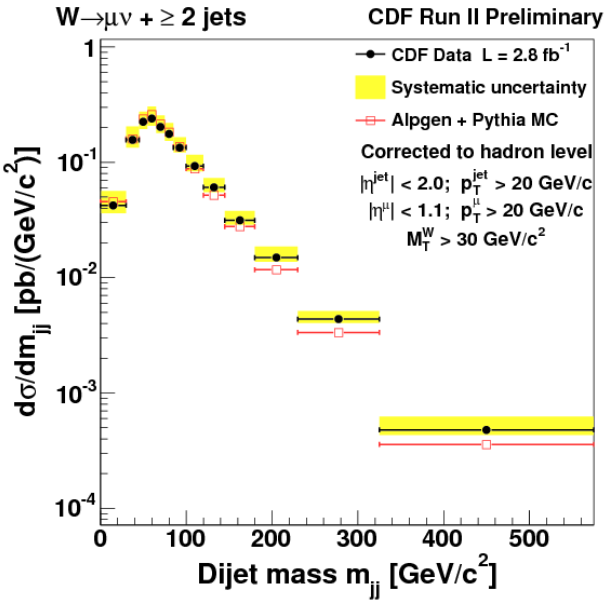

Figure 24: Dijet Mass Cross-section for $W \to \mu\nu + \geq 2$ jets.

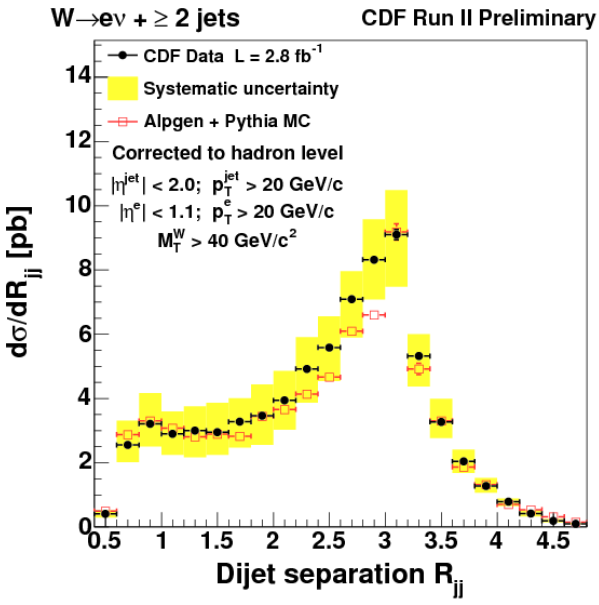

Figure 25: Dijet Separation Cross-section for $W \to e\nu + \geq 2$ jets.

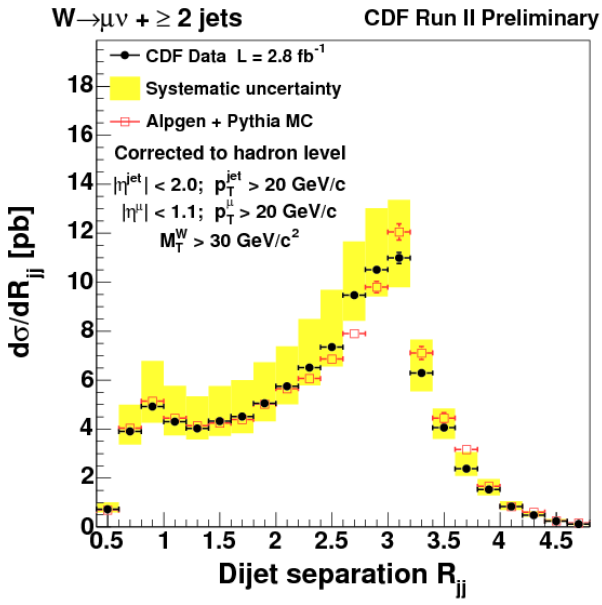

Figure 26: Dijet Separation Cross-section for $W \to \mu\nu + \geq 2$ jets.

Farthest Separated Jet Pseudo-rapidity Difference: $\frac{\mathrm{d}\sigma_n}{\mathrm{d}\Delta\eta}$

We calculate $\Delta\eta = |\eta_a - \eta_b|$ for the farthest two jets in pseudo-rapidity (*not* the leading dijets) for ≥ 2 and ≥ 3 jets. We also form a ratio between the two distributions $r_{\Delta\eta}$ via

$$r_{\Delta\eta} = \frac{\mathrm{d}\sigma_3/\mathrm{d}\Delta\eta}{\mathrm{d}\sigma_2/\mathrm{d}\Delta\eta}$$

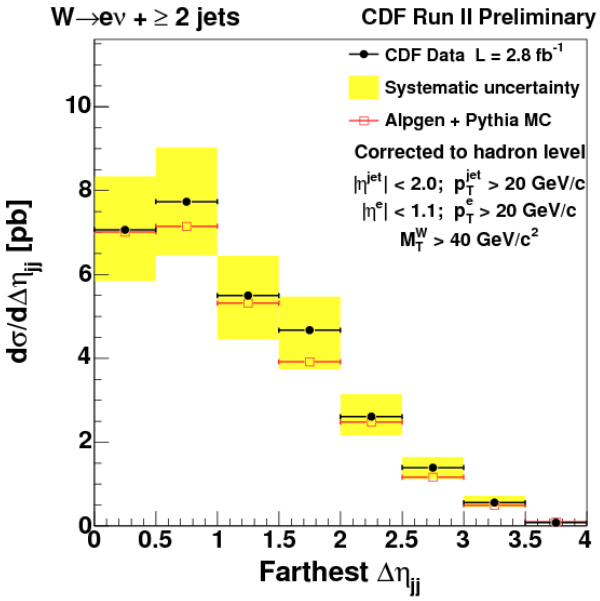

Figure 27: $\Delta\eta$ Cross-section for $W \to e\nu + \geq 2$ jets.

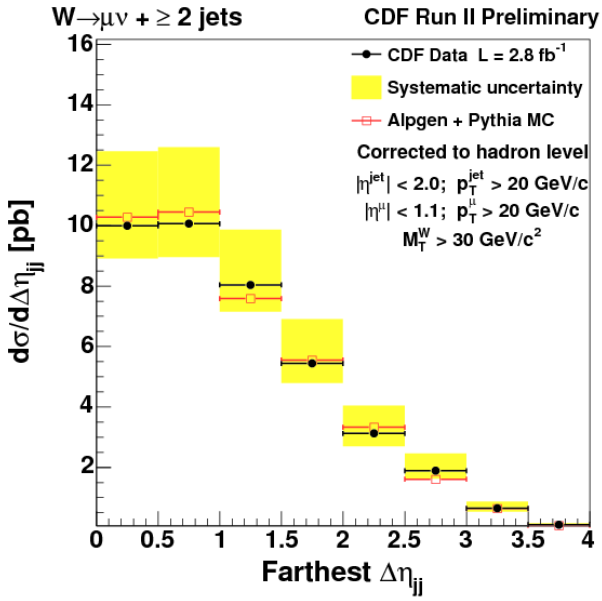

Figure 28: $\Delta\eta$ Cross-section for $W \to \mu\nu + \geq 2$ jets.

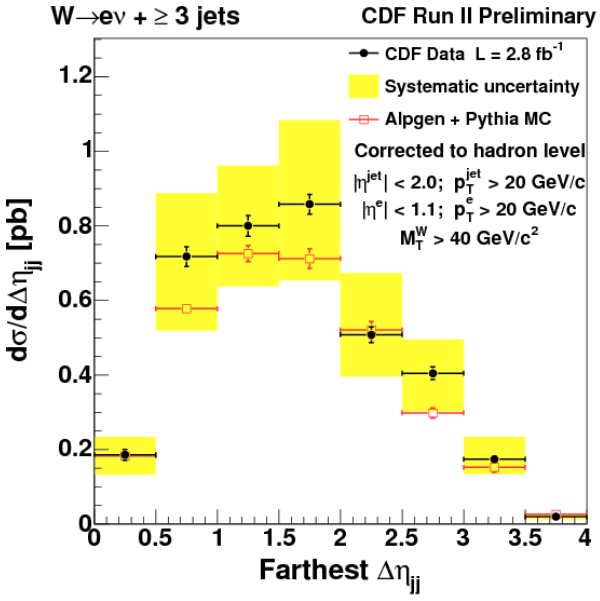

Figure 29: $\Delta\eta$ Cross-section for $W \to e\nu + \geq 3$ jets.

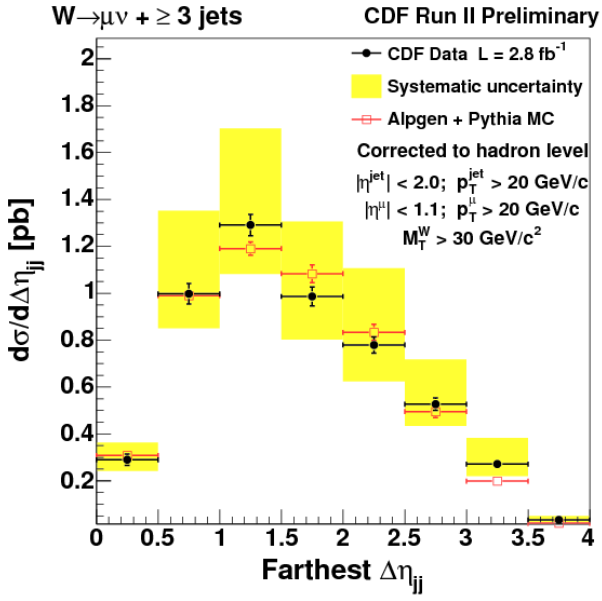

Figure 30: $\Delta\eta$ Cross-section for $W \to \mu\nu + \geq 3$ jets.

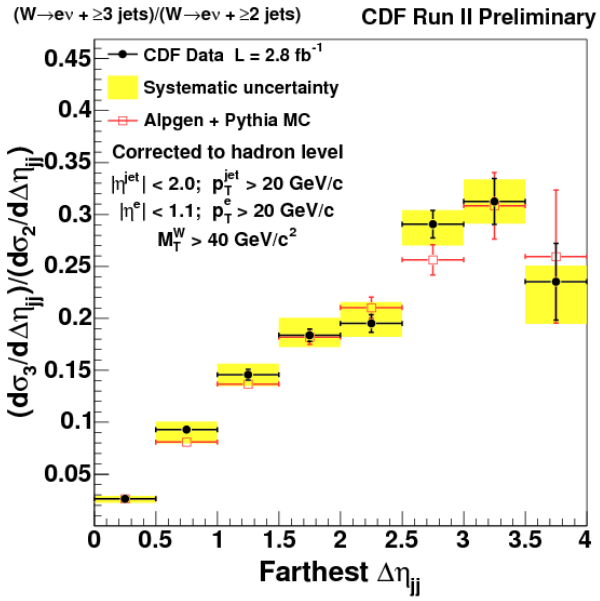

Figure 31: $r_{\Delta\eta}$ Cross-section ratio for $W \to e\nu$ between $\geq$3 and $\geq$2 jets.

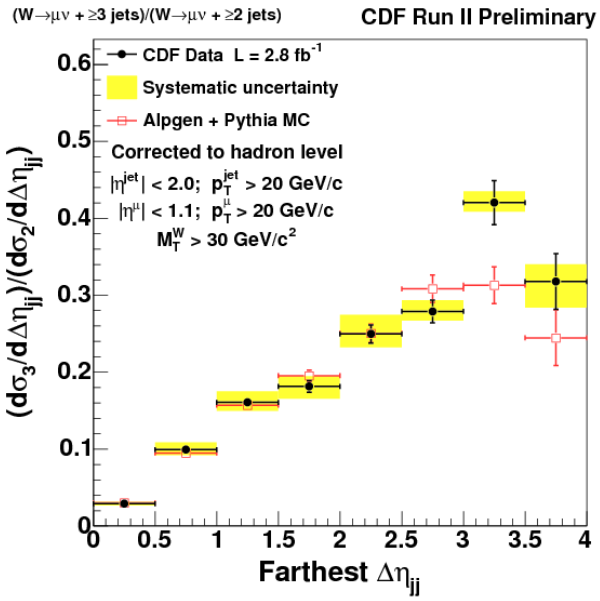

Figure 32: $r_{\Delta\eta}$ Cross-section ratio for $W \to \mu\nu$ between $\geq$3 and $\geq$2 jets.

IX Acknowledgments

We thank R. K. Ellis, J. Campbell, and G. Zanderighi for their help with obtaining NLO theory predictions. We also thank the Fermilab staff and the technical staffs of the participating institutions for their vital contributions. This work was supported by the U.S. Department of Energy and National Science Foundation; the Italian Istituto Nazionale di Fisica Nucleare; the Ministry of Education, Culture, Sports, Science and Technology of Japan; the Natural Sciences and Engineering Research Council of Canada; the National Science Council of the Republic of China; the Swiss National Science Foundation; the A.P. Sloan Foundation; the Bundesministerium für Bildung und Forschung, Germany; the World Class University Program, the National Research Foundation of Korea; the Science and Technology Facilities Council and the Royal Society, UK; the Institut National de Physique Nucleaire et Physique des Particules/CNRS; the Russian Foundation for Basic Research; the Ministerio de Ciencia e Innovación, and Programa Consolider-Ingenio 2010, Spain; the Slovak R&D Agency; and the Academy of Finland.

References

[1] T. Aaltonen *et al.* (CDF Collaboration), Phys. Rev. D **77**, 011108(R) (2008).

[2] R. Blair *et al.* (CDF Collaboration), FERMILAB-PUB-96/390-E (1996).

[3] A. Abulencia, *et al.*, J. Phys. G Nucl. Part. Phys. **34**, (2007).

[4] G. C. Blazey *et al.*, hep-ex/0005012; T. Affolder *et al.* (CDF Collaboration), Phys. Rev. D **64**, 032001 (2001); A. Abulencia *et al.* (CDF Collaboration), Phys. Rev. D **74**, 071103(R) (2006); T. Aaltonen *et al.* (CDF Collaboration), Phys. Rev. D **78**, 052006 (2008).

[5] A. Bhatti *et al.*, Nucl. Instrum. Meth. A **566** 375 (2006).

[6] M. L. Mangano, M. Moretti, F. Piccinini, R. Pittau, and A. Polosa, J. High Energy Phys. 07 (2003) 001.

[7] T. Sjostrand, S. Mrenna, and P. Skands, J. High Energy Phys. 05 (2006) 026.